Shear Stress Initiates Endothelial to Mesenchymal Transition in Endocardial Endothelial Cells

Kathleen N. Brown[1], Hong Kim T. Phan[1], Tasneem Mustafa[1], Elysa Jui[1], Fariha N. Ahmad[1], Ravi P. Birla[2,3], Philippe Sucosky[4], Jennifer P. Connell[1], Sundeep G. Keswani[2,3], and K. Jane Grande-Allen[1]

Affiliations

[1]Department of Bioengineering, Rice University, Houston, TX

[2]Department of Surgery, Baylor College of Medicine, Houston, TX

[3]Division of Pediatric Surgery, Department of Surgery, Texas Children's Hospital, Houston, TX

[4]Department of Mechanical Engineering, Kennesaw State University, Kennesaw, GA

Abbreviated title: Shear stress-driven EndMT in EECs

Address for correspondence:

K. Jane Grande-Allen, Ph.D.

Department of Bioengineering

Rice University

6100 Main St., MS 142

Houston, TX 77005

Phone: 713-348-3704

Email: grande@rice.edu

Abstract

Discrete subaortic stenosis (DSS) is a congenital heart disease characterized by the formation of a fibrotic membrane below the aortic valve. The underlying cellular mechanisms of this disease are currently unknown. As one of the distinguishing features of DSS is the elevated pressure gradient in the left ventricular outflow tract, it is hypothesized that membrane formation is caused by elevated wall shear stress applied to the endocardial endothelial cells (EECs), triggering fibrosis. To correlate shear stress to an EEC fibrotic phenotype, we applied fluid shear stress to EECs at physiological and pathological shear rates using a cone-and-plate device, designed to recapitulate physiological wall shear stress in a controlled in vitro environment. Controlled shear stress regimes were applied to EECs to replicate the conditions observed in DSS patients. We found that elevated shear stress triggered EEC alignment as well as endothelial-to-mesenchymal transformation (EndMT) signaling pathways driven by upregulation of *SNAI1* gene expression. The EECs were then treated with a small molecule inhibitor of Snail1 protein, CYD19, to attempt to attenuate EndMT signaling, and subsequently subjected to pathological shear stress. The Snail1 inhibitor did downregulate selected markers of EndMT signaling, although only transiently. Interestingly, the application of shear stress had a greater effect on the EEC gene and protein expression than did the Snail1 inhibition. This investigation of EEC response to shear stress reveals the pronounced and complex effect of this mechanical stimulation on the EEC phenotype. Further study should reveal the mechanisms that drive fibrosis and the formation of the DSS membrane.

Introduction

Discrete subaortic stenosis (DSS) is a rare, congenital heart disease characterized by formation of a fibrotic membrane in the subvalvular region of the left ventricular outflow tract (LVOT) of the heart, which then obstructs blood flow through the aortic valve. Up to 10% of patients with congenital heart disease present with a LVOT obstruction (1), and DSS accounts for up to 15% of these cases (2). When left untreated, the DSS membrane will continue growing and restrict blood flow through the LVOT, resulting in high rates of morbidity and mortality (3). Currently the only option for treatment is surgical removal of the membrane. Physicians typically wait for the membrane to progress into an “optimal surgical window” (1). However, up to 29% of DSS patients have recurrence of the membrane within 13 years of their first membrane resection (3).

The underlying cellular mechanism that drives membrane formation in DSS is unknown; however, there are clues in the disease presentation. For example, the membrane is composed of fibrotic extracellular matrix proteins and the left ventricular wall of patients with DSS is thickened, both hallmarks of cardiac fibrosis. Additionally, the aortoseptal angle is steeper than normal in patients with DSS, which could contribute to elevated wall shear stress within the LVOT (4–6). In the LVOT, physiological wall shear stresses range from 10-15 dynes/cm^2, and DSS patients experience supra-physiological wall shear stresses that range from 30-55 dynes/cm^2 (1,4,7,9).

The poor understanding of the mechanism of DSS is due in part to the lack of suitable in vitro models. To overcome this limitation, we created an *in vitro* model of DSS by investigating the effects of elevated wall shear stress levels on endocardial endothelial cells (EECs), the cells that line the LVOT. We isolated EECs from porcine hearts, exposed the cells to varying levels of shear stress using a previously reported cone-and-plate device (10), and then characterized the cellular inflammatory and fibrotic responses.

Materials and Methods

Endocardial endothelial cell isolation & culture

Endocardial endothelial cells were isolated from porcine hearts; the hearts of young adult pigs (6-12 months old) are commonly used as an experimental model for human hearts due to their anatomical and structural similarities and convenient availability.[36–38] Cells were cultured on tissue culture treated flasks with Endothelial Growth Medium-2 (EGM-2, Lonza), which was changed every other day until the cells reached ~75% confluence. For experiments, cells were plated in 60 mm tissue culture treated petri dishes (Thermo Fisher) at a density of 0.8 x10^6 cells per dish. The cells were grown to confluency prior to further experimentation.

Applying shear stress with a cone-and-plate device

A cone-and-plate device was used to apply shear stress (**Figure 1**), as previously described (10). The cone and shaft were machined from titanium and the cover from Teflon. The cone had a smooth surface with an angle of 0.5°. The gap height of the cone was adjusted using the collar shaft. The shear stress applied by the cone was determined as $\tau = \mu \cdot \frac{\omega \cdot r}{h_0 + r \cdot \alpha}$, where τ = wall shear stress, μ = dynamic viscosity of fluid, ω = angular velocity of the cone, r = radius of the cone, h_0= gap height, and α = angle between the cone-and-plate, as previously reported (11).

The cones were sterilized via exposure to UV light for a minimum of 3 hours. The gap height of the cone was set by loading the cone onto a petri dish containing two #1 coverslips, stacked atop each other to achieve a gap height of 300 μm, and then tightening the collar shaft. The adjusted cone was then loaded onto a petri dish containing EECs and 2.0 mL of EGM-2. The system was then placed on a magnetic stir plate with a controllable rotational

speed (Cole-Parmer). The shear stress levels used in experiments were static conditions (no shear stress), low shear (15 dynes/cm^2), medium shear (20 dynes/cm^2), or high shear (35 dynes/cm^2). Using the equation above, the desired shear stress was used to determine the required rotational setting of the stir plate, as shown in **Table 1**.

Cell imaging and analysis

Brightfield images of the cells were obtained before and after the application of shear stress, using a Nikon Ti2 eclipse microscope. After image acquisition, cell alignment analysis was performed in ImageJ using the OrientationJ plugin. This plugin produced cell orientation data as well as images of EECs that were overlain with a color map corresponding to the degree of orientation.

Quantitative polymerase chain reaction

Gene expression of key markers of cell phenotype, fibrosis, and inflammation were evaluated following the application of shear stress. Total RNA was isolated from samples by incubating each sample with 300 µL TRIzol reagent (Thermo Fisher) for 10 minutes and then scraping up the cells. The total RNA was then purified using the Direct-zol RNA MicroPrep Kit (Zymo Research) according to manufacturer's instructions. RNA quality and quantity was evaluated using the NanoDrop 2000. RNA samples were stored at -80°C until further processing. cDNA was synthesized from of 200 ng RNA per sample using the High Capacity cDNA Reverse Transcription Kit (Thermo Fisher) per manufacturer's instructions. cDNA samples were then stored at -20˚C. Quantitative reverse transcriptase polymerase chain reaction (qRT-PCR) was performed using the iTaq Universal Probes Supermix (Bio-Rad) with Taqman porcine primers specific to CD31 (probe ID: Ss03392600_u1), ACTA2 (Ss04245588_m1), VCAM1 (Ss03390912_m1), ICAM1 (Ss03392385_m1), Vimentin

(Ss04330801_gH), YAP1 (Ss06912139_m1), von Willebrand Factor (Ss04322692_m1), COL1A2 (Ss03375009_u1), COL3A1 (Ss04323794_m1), and GAPDH (Ss03374854_g1). qPCR for SNAI1 expression was performed using the RT^2 SYBR Green qPCR Mastermix (Qiagen) with RT^2 qPCR Primer Assay porcine primers specific to SNAI1 (GeneGlobe ID: PPS07880A), and GAPDH (PPS00192A). To analyze the PCR results, fold changes were calculated using the $\Delta\Delta$CT method. Briefly, the CT values of experimental conditions were normalized to expression of GAPDH, then normalized to the expression of the control sample.

Fibrosis profiler array

For a more comprehensive analysis of the fibrotic reponse of the EECs to shear stress, we utilized the RT^2 Profiler PCR Array - Pig Fibrosis (Qiagen, Gene GlobeID: PASS-120ZD). RNA samples were isolated and purified as previously described. cDNA was synthesized using the RT^2 First Strand Kit (Qiagen). All kits were used according to manufacturer's instructions. The analysis of this array was performed on the Qiagen website, on the GeneGlobe data analysis tab.

Small molecule inhibition of Snail

To test the role of Snail in mechanotransduction signalling in EECs, a small molecule inhibitor of Snail, CYD19 (Aobious), was applied to cells. CYD19 inhibits Snail1 *in vitro* and *in vivo* with a post-translational modification that promotes degradation of the Snail1 protein through the ubiquitin-proteasome pathway (12). The molecule was dissolved in dimethylsulfoxide (DMSO) and stored at room temperature in a stock solution concentration of 4.0937 μM. CYD19 was added to the cells at a concentration of 50 nM, as recommended by a previous study (12). Cells were treated with CYD19 or the vehicle control (an equivalent

volume of DMSO) for 2 days. The cell culture media was then changed and the cells were treated with static or high shear stress conditions for 1.5 or 24 hours.

Flow cytometry

To evaluate the protein expression of the EECs following the experimental treatments, flow cytometry was performed. The cells were rinsed with phosphate buffered saline (PBS) then incubated with 5 mL of Accutase (Sigma-Aldrich) per 60 mm dish for 10 minutes at 37°C. After incubating, the dishes were gently tapped to lift the cells. The Accutase solution was transferred to a conical tube and then centrifuged for 5 minutes at 150 x*g*. The cells were then resuspended in 1% fetal bovine serum (FBS, Fisher Scientific) in PBS at a density of 1 $x10^6$ cells per 100 µL. The cells were divided into different microcentrifuge tubes for the testing conditions.

For extracellular protein analysis, the antibodies and corresponding isotype controls were added to their respective samples' tubes at concentrations recommended by the manufacturer (see **Table 2**). The samples were protected from light and incubated at room temperature for 15 minutes, then washed twice with 1 mL of 1% FBS in PBS.

For intracellular protein analysis, the cells were fixed in 1 mL of 4% paraformaldehyde at 4˚C for 20 minutes. After fixation, the cells were permeabilized in 1% Tween20, 1% FBS in PBS at room temperature for 15 minutes. The cells were then centrifuged and resuspended in 100 µL of the 1% Tween20, 1% FBS in PBS solution. The antibodies and corresponding isotype controls were then added at concentrations recommended by the manufacturer (**Table 2**). The samples were protected from light and incubated with the antibody at room temperature for 45 minutes, then washed with 1 mL of 1% FBS in PBS.

The stained cells were resuspended in 500 μL 1% FBS in PBS and transferred to polystyrene 5 mL flow cytometry tubes (MTC Bio). Flow cytometry was performed on a Sony MA900 flow cytometer, and analysis was performed in FlowJo Version 7.

Statistical analysis

Statistical analysis was performed in GraphPad Prism Version 9.4.1. For most of the experiments, a one-way ANOVA test was performed, with post-hoc analysis performed using Tukey's test. All data was graphed as means $\pm$ standard deviation. For the small molecule inhibitor experiments, a two-way ANOVA was performed, with post-hoc analysis performed using Tukey's test. Results with $p < 0.05$ were considered statistically significant. Comparisons with p-values between 0.05-0.15 were considered as non-significant trends.

Results

Shear stress drives EEC alignment

After the experimental period, brightfield images of the EECs were captured at multiple locations around the dish, and we analyzed the distribution of orientation of 10 samples for each shear condition. We observed that after application of shear stress, the cells aligned to the direction of the fluid rotation (**Figure 2).** In the static condition, the cells had a non-uniform distribution of alignment. After applying low (15 dynes/cm^2) or medium (20 dynes/cm^2) magnitudes of shear stress, the cells aligned in a more uniform direction. Interestingly, in the high shear stress condition (35 dynes/cm^2), the cells displayed a non-uniform alignment, similar to the static condition.

Shear stress drives time dependent gene expression

We used qRT-PCR to analyze the gene expression of the EECs in response to varying shear rates over time (**Figure 3)**, examining *CD31 and ACTA2* as representative endothelial and fibrotic markers, respectively, and *ICAM1* and *VCAM1* as representative inflammatory markers. The resulting cellular response was dependent on shear rate in a way that differed between time points. *CD31* remained largely unchanged across time points and shear conditions, indicating that the cells maintained an endothelial phenotype. *ACTA2*, which encodes for the protein α-smooth muscle actin, was downregulated in response to shear at all magnitudes, but only at the 8-hour time point. The inflammatory marker, *ICAM1* was upregulated at the 1.5-hour time point in response to shear, but did not demonstrate differences at later time points, other than a slight trend of a reduction with shear at 8 hours. In contrast, *VCAM1* was downregulated by all shear magnitudes at both later time points. At 16 hours, however, this reduction in *VCAM1* expression was most pronounced for the lower shear conditions (15-20 dyn/cm^2).

Fibrosis array suggests role for Snail in shear stimulated EECs

Based on these initial findings of cellular response to shear stress, we used a PCR profiler array to analyze expression of 84 fibrosis-related genes in either static or high shear stress (35 dynes/cm^2) conditions at 3 time points. The focus on the high shear stress condition was based on physiological measurements in DSS and on how this condition demonstrated the greatest changes in *ACTA2*, *ICAM1*, and *VCAM1* expression. Overall, the fibrosis array found that more genes were upregulated than downregulated in response to shear stress (**Supplemental Figure 1**). The heat map of the profiler array showed that there was consistency of gene expression within each experimental group, but that the expression profiles changed over time, supporting the PCR results (**Figure 4)**.

The genes that were strongly upregulated or downregulated in response to shear stress provided insight into the involvement of specific signaling pathways. *SNAI1*, which encodes for the transcription factor Snail1, was very strongly upregulated (26.6 fold change (FC), $p < 0.01$) at the earliest time point of 1.5 hours, whereas ECM genes such as *COL3A1* (183.81 FC, $p=0.001$), *COL1A2* (38.86 FC, $p=0.015$), and *DCN* (90.73 FC, $p=0.031$) were significantly upregulated at the later time point of 16 hours (**Table 3**). Several other genes relevant to ECM, cell-matrix adhesion, and fibrosis were also upregulated significantly for at least one of the later time points, including *ITGB3* (8.0-14.8 FC), *TFGB1* (2.8-2.9 FC), *TGFB3* (4.7 FC), *MMP14* (2.1-2.8 FC), and *TIMP1* (11.3-15.3 FC, all $p<0.05$). In contrast, selected signaling factors with an endothelial role, such as *CTGF* (-2.5 FC) and *CCL11* (-4.3 to -11.1 FC), were significantly downregulated ($p<0.05$). Based on this data, we hypothesized that *SNAI1* was a mechanosensitive marker that was upregulated at early time points in response to shear. We speculated that this then initiated signaling pathways that lead to the increased ECM genes observed at later time points, which were indicative of endothelial-to-mesenchymal transition (EndMT).

Small molecule inhibition of Snail transiently influenced EndMT markers

To investigate this hypothesis, cells were treated with CYD19, which inhibits Snail1 via a post-translational modification (12), prior to the application of high shear stress. We observed an initial shift in cell morphology between the CYD19-treated and the vehicle-treated cells, as shown in **Figure 5A.** The vehicle-treated EECs had a very similar elongated and swirling morphology to the EECs shown in previous figures, whereas the CYD19-treated EECs became more round and cobblestone-like.

At 1.5 hours after the application of shear stress, the gene expression of *SNAI1* appeared to be greater in the untreated group (**Figure 5B**), consistent with the fibrosis PCR

assay data, although this difference was not statistically significant due to a high data spread. Treatment with CYD19 did not significantly change the gene expression of *SNAI1* in either of the static or high shear stress conditions, which was expected since CYD19 inhibits Snail1 on the protein level. The magnitude of difference between the static and high shear group appeared lessened in the CYD19 treated samples. In contrast with gene expression, at 1.5 hours Snail1 protein expression in the static cultured EECs was downregulated in response to CYD19 treatment compared to untreated (vehicle) controls. Interestingly, protein levels of Snail1 were decreased in response to high shear stress in the vehicle control groups. By 24 hours, *SNAI1* gene expression was not affected by either CYD19 treatment or the application of shear stress. Furthermore, Snail1 protein expression was abundant across all of the samples at the 24 hour time point (70-80%) compared to the expression level at 1.5 hours (10-40%).

At 1.5 hours, high shear stress reduced the protein expression of two mesenchymal phenotypic markers, α-smooth muscle actin (α-SMA) and vimentin (**Figure 6A-B**). At this timepoint, CYD19 treatment caused a slight reduction in vimentin protein for the statically cultured EECs (p=0.054, trend). Otherwise, at 1.5 hours CYD19 treatment had no effect on protein expression for these two markers, and neither factor had a significant effect on *ACT2* or *VIM* gene expression. At 24 hours, high shear stress downregulated *ACTA2* gene expression, α-SMA protein expression, and VIM gene expression. Again, there was no significant effect of CYD19 treatment on expression levels, although there was a trend of reduced α-SMA protein in the statically cultured EECs (p=0.0709). It was noteworthy that, in all groups, more cells were positive for α-SMA protein at 24 hours ((20-60%) than at 1.5 hours (1-3%). Similarly, vimentin protein expression was uniformly strong in all groups at 24 hours (<90%) compared to the protein expression levels at 1.5 hours (40-80%).

In contrast to the mesenchymal markers, gene expression of the inflammatory marker *VCAM1* at 1.5 hours was upregulated in response to CYD19 treatment, and was downregulated in response to high shear stress (**Figure 6C**). At 24 hours, *VCAM1* gene expression was downregulated in response to high shear stress, but not affected by CYD19. VCAM1 protein expression was not influenced by CYD19 treatment at either timepoint, but there were trends of reduced VCAM1 protein expression in the untreated groups following high shear stress for 1.5 hours (p=0.1563) and 24 hours (p=0.0908).

Finally, the gene expression of endothelial marker *CD31* at 1.5 hours was downregulated in response to shear stress (**Figure 6D**). At this timepoint, CYD19 did not affect *CD31* gene expression but did cause a slight non-significant trend of greater CD31 protein expression (p=0.1077). At 24 hours, *CD31* gene expression was downregulated by CYD19 treatment and downregulated by exposure to high shear stress. The protein expression of CD31 at this later timepoint was upregulated by both the CYD19 treatment and the application of high shear stress (p=0.0975, trend for CYD19-treated). In contrast to the expression levels of mesenchymal protein markers between timepoints, CD31 protein expression was notably lower at the 24 hour time point (30-65%) than at the 1.5 hour time point (70-90%).

Discussion

The altered subaortic anatomy found in discretre subaortic stenosis affects the local blood flow and consequently the magnitude of shear stresses that are experienced by the endocardial endothelial cells in the LVOT. In an effort to mimic the disease pathologies observed in DSS, we applied physiological and pathological levels of wall shear stress to EECs and characterized the cellular response through alignment, gene expression, and protein expression. The main findings of these experiments were that first, the EECs were mechanoresponsive and aligned in response to low and medium magnitudes of shear stress,

but the collective alignment of EECs in response to high shear stress was more complex. Second, with increasing duration of exposure to high shear stresses, there was increased gene expression of many factors related to EndMT, especially those relevant to ECM remodeling, cell-matrix adhesion, and other mesenchymal markers. Third, the use of the CYD-19 inhibitor was effective in inhibition of Snail1 protein and mesenchymal transition, but the effects of this inihibitor were only transient and frequently overshadowed by the effects of high shear stress.

The EECs demonstrated that they were mechanosensitive by adjusting their alignment in response to shear, yet this realignment occurred in a shear magnitude-dependent manner. When comparing the low shear, medium shear, and high shear graphs, the cellular alignment is similar, with the most uniformity in cell alignment found in the medium shear condition. The shear-driven alignment of the EECs in low and medium shear rates is a phenomenon that has been observed in many studies where shear stress is applied to endothelial cells. However, after applying high shear stress to EECs, the condition most closely mimicking the disease state observed in DSS, the alignment of cells were not as impacted by the application of shear stress; we speculate that the EECs were transitioning to a mesenchymal phenotype, such as a fibroblast or myofibroblast.

The application of high shear stresses to the EECs resulted in the expression of many early- and late-stage genes involved in endothelial to mesenchymal transition (EndMT). During the EndMT process, the endothelial cells lose their endothelial characteristics, and begin to express mesenchymal markers (13,14,16,17,21). The transition is a continuum, and endothelial cells undergoing EndMT co-express both endothelial and mesenchymal markers (13,18,19), although this co-expression can vary depending on the pathological environment and cell type (14–16,18,19). In this study, a link between high shear stress and EndMT was shown throughout the culture duration. EECs exposed to 1.5 hours of high shear stress

upregulated genes related to transcription factors, growth factors, cytokines, chemokines, and the formation of a transitional extracellular matrix (ECM). By the 16 hour timepoint, the EECs experiencing high shear stress showed strongly upregulated gene expression of mesenchymal markers, ECM, and matrix remodeling enzymes such as ACTA2, collagens 1 and 3, decorin, β3 integrins, MMP14, TIMP1, and TGFβ1, all markers of late EndMT processes (13–15,18,19). At the same time, high shear stress caused down-regulation of vascular endothelial markers such as CTGF. This effect of time, as well as shear stress magnitude, on the response of the EECs was evident in the initial PCR analysis as well as the fibrosis gene array. The high shear stress also caused a dramatic increase in expression of the transcription factor Snail1, an important regulator of EndMT (13,22,17,19,20,23–26). Therefore, we sought to determine if blocking Snail1 could inhibit development of EndMT in EECs using CYD19, a small molecule inhibitor of Snail1 protein post-translational modification.

Inhibition of Snail1 post-translational modification was able to dampen EndMT by EECs transiently. Since the inhibitor affected the Snail1 protein, the strongest effect on Snail1 expression was observed at the protein level, although this was only at the early time point. At this time (1,5 hours), the Snail1 inhibition maintained a more endothelial, less mesenchymal phenotype in the statically cultured EECs as shown by trends of reduced vimentin and increased CD31 and a strong, significant increase in *VCAM1*. By 24 hours, the inhibitor had no effect on Snail1 expression at either the gene or protein level. Other than a trend of slightly reduced α-SMA protein expression in the CYD19 treated group, which may be a downstream remnant of the Snail1 inhibition, there was no effect of CYD19 treatment on the mesenchymal or inflammatory genes at 24 hours. In contrast, CD31 expression was affected by CYD19 treatment at 24 hours, with slightly lower gene expression but slightly greater protein expression. When the magnitudes of protein expression were considered collectively, the EECs at 24 hours appeared more mesenchymal and less endothelial in their phenotypic

characteristics, especially in the statically cultured groups. Thus, the CYD19 small molecular inhibition of Snail1 activity and EndMT appeared to be successful, but this effect was only broadly evident for a limited time.

Interestingly, the effects of high shear stress were much more pronounced than that of the small molecule Snail1 inhibitor. This effect of high shear was particularly evident for *VCAM1* expression at both time points, as well as early protein expression and late gene expression for both α-SMA and vimentin, regardless of Snail1 inhibition. These *VCAM1* and *ACTA2* responses were consistent with the 8 hour EEC responses to shear stress in the initial PCR study. These mechanobiological trends highlight the importance of investigating shear stress when modeling diseases of the heart and cardiovascular system, and also emphasize the challenges of inhibiting the complex cell signaling pathways that drive DSS formation.

This is the first study to apply supra-physiological levels of wall shear stress to EECs and characterize their response as related to DSS formation. EECs have been implicated in several cardiac diseases, yet shear stress studies have focused primarily on modeling the behavior of HUVECs in response to pathological shear rates (20,27). EECs have a unique endothelial phenotype, as shown through proteomic analyses documenting that EECs express a different phenotype from aortic endothelial cells and even vary their phenotype throughout the regions of the heart (28–30). It is well understood that abnormal shear stress induces EndMT in HUVECs and in aortic valve endothelial cells, and may contribute to vascular disease formation (15,18,23,31–36). However, additional studies are needed to gain further infight into the EEC response to pathological shear stress. In a recent study investigating the role of shear stress in the formation of endocardial fibroelastosis (EFE) (20), EECs exposed to abnormal shear conditions showed signs of undergoing EndMT through the co-expression of endothelial and mesenchymal markers and the increased expression of Snail1, which they

concluded contributes to EFE (20). This important work emphasizes that the specific phenotype and resulting signaling pathways of EECs are unique.

These results have provided novel insights into the EEC-specific responses to physiological and pathological levels of shear stress, but they should be considered in the appropriate experimental context. Although we used the recommended dose of CYD19, it will be important in the future to investigate dose dependent effects of the inhibitors of EndMT signaling (12). It is also likely that to recapitulate the full EndMT signaling process that accompanies DSS, additional cell types (such as cardiac fibroblasts and immune cells) would need to be included in the disease model. Additionally, while we investigated the cellular response to shear stress between 1.5 hours and 24 hours, it would be worthwhile to extend these experiments to longer time points to understand the time dependent nature of EndMT progression. Clearly, further investigation is required to uncover the complex signaling mechanisms of the fibrotic membrane formation observed in DSS.

Conclusions

In summary, this study demonstrated that endocardial endothelial cells are highly sensitive to shear stresses and respond by changing their alignment and their gene expression of key markers of cell phenotype, EndMT, and inflammation. Although inhibition of Snail1 with CYD19 had a modest inhibitory effect on EndMT and caused a significant increase in *VCAM1* expression, this effect was largely limited to the earlier timepoint of 1.5 hours. The results provide an important characterization of the EEC response to elevated wall shear stress, and lay the groundwork for additional studies to elucidate how shear stress and EndMT contribute to the role of EECs in DSS and other LVOT pathologies.

Acknowledgements

Financial support for this research was provided by a gift from Lew and Laura Moorman, NIH R01 HL140305 (to KJGA and SGK), and NSF Graduate Research Fellowship Program (for KNB).

References

1. Darcin OT, Yagdi T, Atay Y, Engin C, Levent E, Buket S, et al. Discrete Subaortic Stenosis. Tex Heart Inst J. 2003;30(4):286–92.
2. Allen HD. Moss and Adams' Heart Disease in Infants, Children, and Adolescents. 9th ed. Vol. I&II. Wolters Kluwer; 2016.
3. Donald JS, Naimo PS, d'Udekem Y, Richardson M, Bullock A, Weintraub RG, et al. Outcomes of Subaortic Obstruction Resection in Children. Heart, Lung and Circulation. 2017 Feb 1;26(2):179–86.
4. Shar JA, Brown KN, Keswani SG, Grande-Allen J, Sucosky P. Impact of Aortoseptal Angle Abnormalities and Discrete Subaortic Stenosis on Left-Ventricular Outflow Tract Hemodynamics: Preliminary Computational Assessment. Front Bioeng Biotechnol. 2020;8:114.
5. Yap SC, Roos-Hesselink JW, Bogers AJJC, Meijboom FJ. Steepened aortoseptal angle may be a risk factor for discrete subaortic stenosis in adults. International Journal of Cardiology. 2008 May;126(1):138–9.
6. Cape EG, VanAuker MD, Sigfússon G, Tacy TA, del Nido PJ. Potential Role of Mechanical Stress in the Etiology of Pediatric Heart Disease: Septal Shear Stress in Subaortic Stenosis. Journal of the American College of Cardiology. 1997 Jul;30(1):247–54.
7. Silbiger J. The Role of Shear Stress in the Pathogenesis of Discrete Subaortic Stenosis: Implications for Surgical Treatment. J Heart Valve Dis. 2011;20(2):123–8.
8. Foker JE. Outcomes and Questions About Discrete Subaortic Stenosis. Circulation. 2013 Apr 9;127(14):1447–50.
9. Butany J, Vaideeswar P, David TE. Discrete subaortic membranes in adults—a clinicopathological analysis. Cardiovascular Pathology. 2009 Jul;18(4):236–42.

10. Heo KS, Lee H, Nigro P, Thomas T, Le NT, Chang E, et al. PKCζ mediates disturbed flow-induced endothelial apoptosis via p53 SUMOylation. J Cell Biol. 2011 May 30;193(5):867–84.
11. Sucosky P, Padala M, Elhammali A, Balachandran K, Jo H, Yoganathan AP. Design of an Ex Vivo Culture System to Investigate the Effects of Shear Stress on Cardiovascular Tissue. Journal of Biomechanical Engineering. 2008;130(3):035001.
12. Li HM, Bi YR, Li Y, Fu R, Lv WC, Jiang N, et al. A potent CBP/p300-Snail interaction inhibitor suppresses tumor growth and metastasis in wild-type p53-expressing cancer. Sci Adv. 2020 Apr 22;6(17):eaaw8500.
13. Goncharov NV, Popova PI, Avdonin PP, Kudryavtsev IV, Serebryakova MK, Korf EA, et al. Markers of Endothelial Cells in Normal and Pathological Conditions. Biochem Moscow Suppl Ser A. 2020 Jul 1;14(3):167–83.
14. Kovacic JC, Dimmeler S, Harvey RP, Finkel T, Aikawa E, Krenning G, et al. Endothelial to Mesenchymal Transition in Cardiovascular Disease: JACC State-of-the-Art Review. J Am Coll Cardiol. 2019 Jan 22;73(2):190–209.
15. Dejana E, Hirschi KK, Simons M. The molecular basis of endothelial cell plasticity. Nat Commun. 2017 Feb 9;8(1):14361.
16. Gong H, Lyu X, Wang Q, Hu M, Zhang X. Endothelial to mesenchymal transition in the cardiovascular system. Life Sciences. 2017 Sep 1;184:95–102.
17. Alvandi Z, Bischoff J. Endothelial-Mesenchymal Transition in Cardiovascular Disease. Arterioscler Thromb Vasc Biol. 2021 Sep;41(9):2357–69.
18. Islam S, Boström KI, Di Carlo D, Simmons CA, Tintut Y, Yao Y, et al. The Mechanobiology of Endothelial-to-Mesenchymal Transition in Cardiovascular Disease. Front Physiol. 2021;12:734215.

19. Peng Q, Shan D, Cui K, Li K, Zhu B, Wu H, et al. The Role of Endothelial-to-Mesenchymal Transition in Cardiovascular Disease. Cells. 2022 Jun 3;11(11):1834.
20. Oh NA, Hong X, Doulamis IP, Meibalan E, Peiseler T, Melero-Martin J, et al. Abnormal Flow Conditions Promote Endocardial Fibroelastosis Via Endothelial-to-Mesenchymal Transition, Which Is Responsive to Losartan Treatment. JACC Basic Transl Sci. 2021 Dec;6(12):984–99.
21. Dahal S, Huang P, Murray BT, Mahler GJ. Endothelial to mesenchymal transformation is induced by altered extracellular matrix in aortic valve endothelial cells. J Biomed Mater Res. 2017 Oct;105(10):2729–41.
22. Feulner L, van Vliet PP, Puceat M, Andelfinger G. Endocardial Regulation of Cardiac Development. J Cardiovasc Dev Dis. 2022 Apr 19;9(5):122.
23. Mahler GJ, Frendl CM, Cao Q, Butcher JT. Effects of shear stress pattern and magnitude on mesenchymal transformation and invasion of aortic valve endothelial cells: Shear Stress Induced EndMT. Biotechnol Bioeng. 2014 Nov;111(11):2326–37.
24. Mahmoud MM, Serbanovic-Canic J, Feng S, Souilhol C, Xing R, Hsiao S, et al. Shear stress induces endothelial-to-mesenchymal transition via the transcription factor Snail. Sci Rep. 2017 13;7(1):3375.
25. Zhang H, Lui KO, Zhou B. Endocardial Cell Plasticity in Cardiac Development, Diseases and Regeneration. Circulation Research. 2018 Mar 2;122(5):774–89.
26. Baulida J, Díaz VM, Herreros AG de. Snail1: A Transcriptional Factor Controlled at Multiple Levels. J Clin Med. 2019 May 28;8(6):E757.
27. McCormick ME, Manduchi E, Witschey WRT, Gorman RC, Gorman JH, Jiang YZ, et al. Spatial phenotyping of the endocardial endothelium as a function of intracardiac hemodynamic shear stress. J Biomech. 2017 Jan 4;50:11–9.

28. Aneesh Kumar A, Ajith Kumar GS, Satheesh G, Surendran A, Chandran M, Kartha CC, et al. Proteomics Analysis Reveals Diverse Molecular Characteristics between Endocardial and Aortic-Valvular Endothelium. Genes (Basel). 2021 Jun 30;12(7):1005.
29. Jaleel A, Aneesh Kumar A, Ajith Kumar GS, Surendran A, Kartha CC. Label-free quantitative proteomics analysis reveals distinct molecular characteristics in endocardial endothelium. Mol Cell Biochem. 2019 Jan;451(1–2):1–10.
30. McCormick ME, Manduchi E, Witschey WRT, Gorman RC, Gorman JH, Jiang Y, et al. Integrated Regional Cardiac Hemodynamic Imaging and RNA Sequencing Reveal Corresponding Heterogeneity of Ventricular Wall Shear Stress and Endocardial Transcriptome. J Am Heart Assoc [Internet]. 2016 Apr 18 [cited 2018 Jul 4];5(4). Available from: https://www.ncbi.nlm.nih.gov/pmc/articles/PMC4859290/
31. Moonen JRAJ, Lee ES, Schmidt M, Maleszewska M, Koerts JA, Brouwer LA, et al. Endothelial-to-mesenchymal transition contributes to fibro-proliferative vascular disease and is modulated by fluid shear stress. Cardiovasc Res. 2015 Dec 1;108(3):377–86.
32. Ajami NE, Gupta S, Maurya MR, Nguyen P, Li JYS, Shyy JYJ, et al. Systems biology analysis of longitudinal functional response of endothelial cells to shear stress. Proc Natl Acad Sci U S A. 2017 Oct 10;114(41):10990–5.
33. Serbanovic-Canic J, Souilhol C, Evans PC. Shear stress makes its mark on the endothelial genome. Cardiovasc Res. 2019 Aug 1;115(10):1449–51.
34. Silvani G, Romanov V, Cox CD, Martinac B. Biomechanical Characterization of Endothelial Cells Exposed to Shear Stress Using Acoustic Force Spectroscopy. Frontiers in Bioengineering and Biotechnology [Internet]. 2021 [cited 2022 Oct 29];9. Available from: https://www.frontiersin.org/articles/10.3389/fbioe.2021.612151

35. Maurya MR, Gupta S, Li JYS, Ajami NE, Chen ZB, Shyy JYJ, et al. Longitudinal shear stress response in human endothelial cells to atheroprone and atheroprotective conditions. Proceedings of the National Academy of Sciences. 2021 Jan 26;118(4):e2023236118.
36. Li Af, Tan L, Zhang S, Tao J, Wang Z, Wei D. Low shear stress-induced endothelial mesenchymal transformation via the down-regulation of TET2. Biochemical & Biophysical Research Communications. 2021 Mar 19;545:20–6.

Table 1. Cone-and-plate Device Settings

Rotational Speed Setting (RPM)	**Shear Stress Applied** (dynes/cm^2)
280	15
370	20
660	35

Table 2. Antibody information and concentrations used for flow cytometry.

Antibody Information	**Amount of Antibody Added to 100 μL Sample**
Extracellular Proteins	
CD31 Monoclonal Antibody (LCI-4) [APC] – Thermo Fisher, #MA5-16769	10 μL
Mouse IgG1 kappa Isotype Control [APC] – Thermo Fisher, #17-4714-42	5 μL
VCAM-1 Monoclonal Antibody (1.G11B1) [FITC] – Thermo Fisher, #MA5-16430	4 μL
Igg1, K Mouse, Clone: P3.6.2.8.1, Isotype Control [FITC] – Thermo Fisher, #11-4714-42	4 μL
CD62E/CD62P Monoclonal Antibody (1.2B6) [PE] – Thermo Fisher, #MA5-28649	4 μL
Mouse IgG1 Isotype Control [PE] – Thermo Fisher, #MA518097	4 μL
Intracellular Proteins	
Snail Antibody [AlexaFluor® 750] – Novus Biologicals, # NBP2-27293AF750	4 μL
Rabbit IgG Isotype Control [AlexaFluor 750] – Novus Biologicals, # NBP2-24891AF750	4 μL
Vimentin Antibody (RV203) [PerCP] – Novus Biologicals, # NBP1-97671PCP	4 μL
Mouse IgG1 Isotype control [PerCP] – Novus Biologicals, # IC002C	4 μL
α-Smooth Muscle Actin Antibody [AlexaFluor 405] – Novus Biologicals, # NBP2-34522AF405	4 μL
Mouse IgG2a Isotype Control (M2AK) [AlexaFluor 405] – Novus Biologicals, # NBP1-96981AF405	4 μL

Table 3. Significantly upregulated or downregulated fibrotic gene expression by EECs experiencing high shear stress (35 dyn/cm^2) relative to the static culture (no shear stress) for 1.5, 8, or 16 hours.

1.5 hours			8 hours			16 hours		
Gene Symbol	**Fold Regulation**	**p-Value**	**Gene Symbol**	**Fold Regulation**	**p-Value**	**Gene Symbol**	**Fold Regulation**	**p-Value**
SNAI1	26.6	0.001352	TIMP1	15.17	0.007376	COL3A1	183.81	0.001261
SMAD7	25.54	0.00695	1TGB3	14.81	0.000275	DCN	90.73	0.031496
JUN	7.95	0.002424	SMAD7	9.7	0.032216	COL1A2	38.86	0.014502
CCL2	5.38	0.004813	IL1A	8.3	0.030976	LOC1006-27243	15.14	0.000107
TNF	5.18	0.003202	SNAI1	7.6	0.014473	TIMP1	11.32	0.020287
EGF	4.96	0.020138	PLAU	5.05	0.032809	ITGB3	8.02	0.002018
INHBE	4.76	0.048119	LOC1005-17053	3.53	0.00042	TGBF2	4.71	0.032484
FASLG	3.32	0.002393	TGFB1	2.93	0.020816	ACTA2	2.81	0.000603
TGIF1	3.09	0.000093	MMP14	2.78	0.022457	TGFB1	2.76	0.000298
PLAT	3.04	0.008234	PLAT	2.48	0.00087	SERPINE1	2.6	0.013912
MYC	2.95	0.046039	TGIF1	2.18	0.005368	SMAD7	2.46	0.034339
PLAU	2.8	0.013067	CTGF	-2.5	0.017989	THBS1	2.22	0.018209
SMAD6	2.33	0.049408	TIMP2	-2.74	0.041479	TGIF1	2.14	0.000343
SERPINE1	2.07	0.008814	ITGA1	-4.06	0.005391	MMP14	2.07	0.014138
ITGA2	2.05	0.010713	CCL11	-11.11	0.003605	MYC	-2.31	0.035862
TIMP1	2.02	0.003785				ACTG1	-2.48	0.017117
TGFB1	2.01	0.001592				ITGA2	-3.11	0.001401
IL1B	-2.57	0.021839				CCL11	-4.33	0.019946
CTGF	-2.59	0.001949				ITGA1	-9.85	0.002572

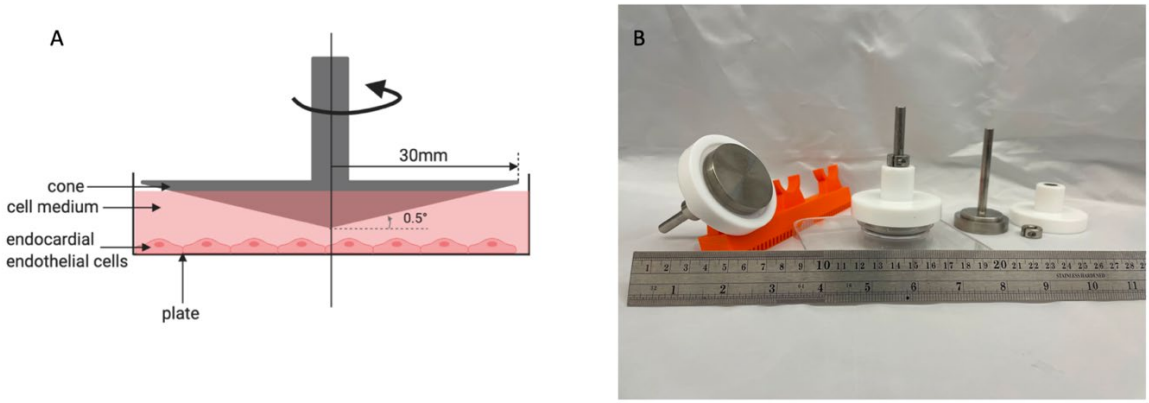

Figure 1. Cone-and-plate Device. (A) Illustration of the cone-and-plate device. Endocardial endothelial cells are grown in a monolayer in a 60 mm petri dish, and the cone is loaded onto the petri dish containing the cells and cell culture medium and rotated using a controllable magnetic stir plate. (B) Photo of the cone and Teflon cover setup used in the shear stress studies. On the left of the photo, the cone is supported by a 3D printed holding device, which is used to position multiple cones towards a UV light for sterilization prior to use. In the center of the photo, the cone is loaded onto a petri dish. On the right of the photo, the cone, Teflon cover, and shaft collar are disassembled to show the individual parts used in the setup.

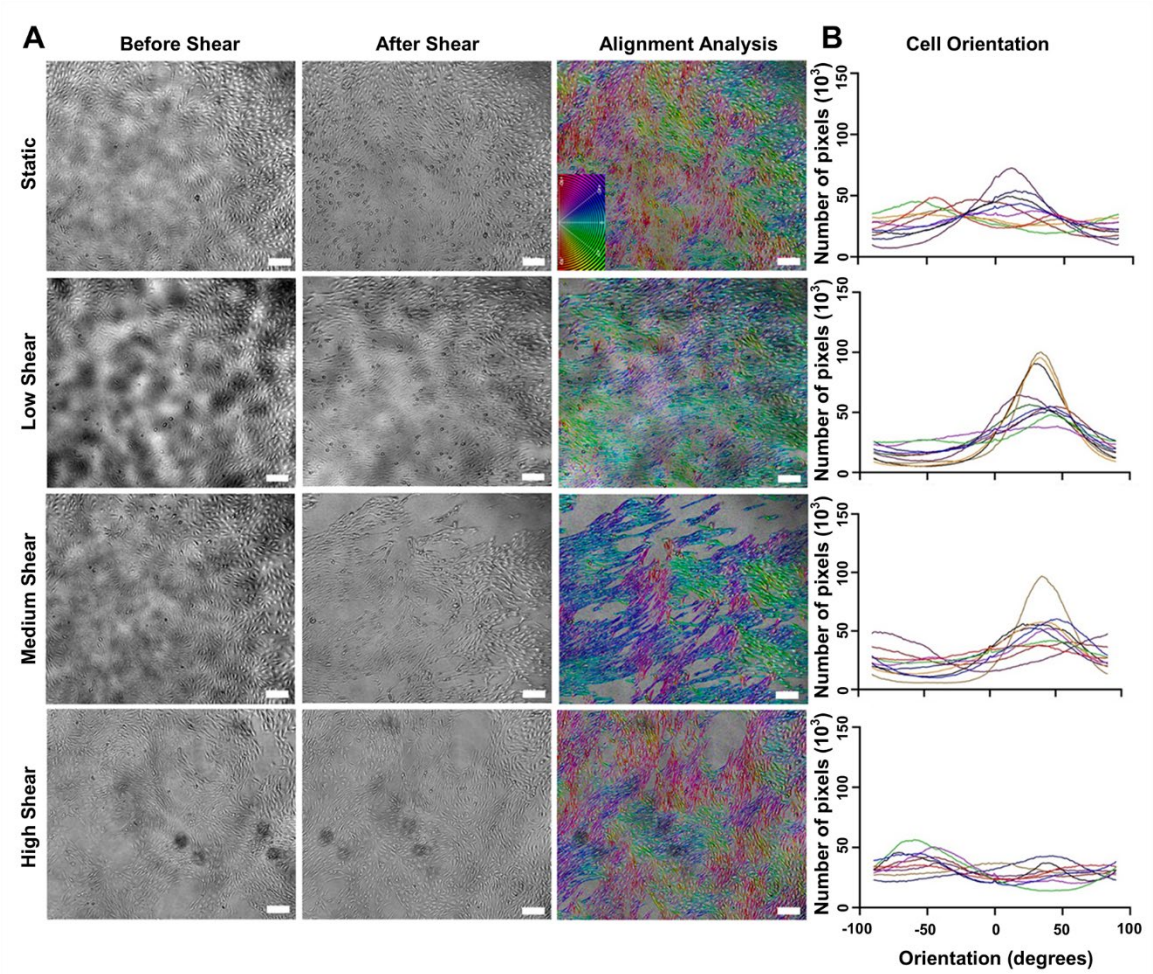

Figure 2. (A) Representative brightfield images of EECs before and after exposure to shear stress. The rows compare EECs exposed to static conditions and low, medium, and high shear stresses. The last column of the panel shows the color mapping of EECs to measure their alignment after exposure to shear stress. The color map code (see inset of static condition) is provided to show how the alignment of the cells corresponds to color and thereby orientation. Scale bar = 200 μm. These were individual samples analyzed at the same location on the petri dish. **(B)** The cell orientation of 10 representative samples of imaged EECs was analyzed for each shear condition to compare their distribution of orientation across shear rates. Each line represents an individual sample analyzed at the same location on the petri dish.

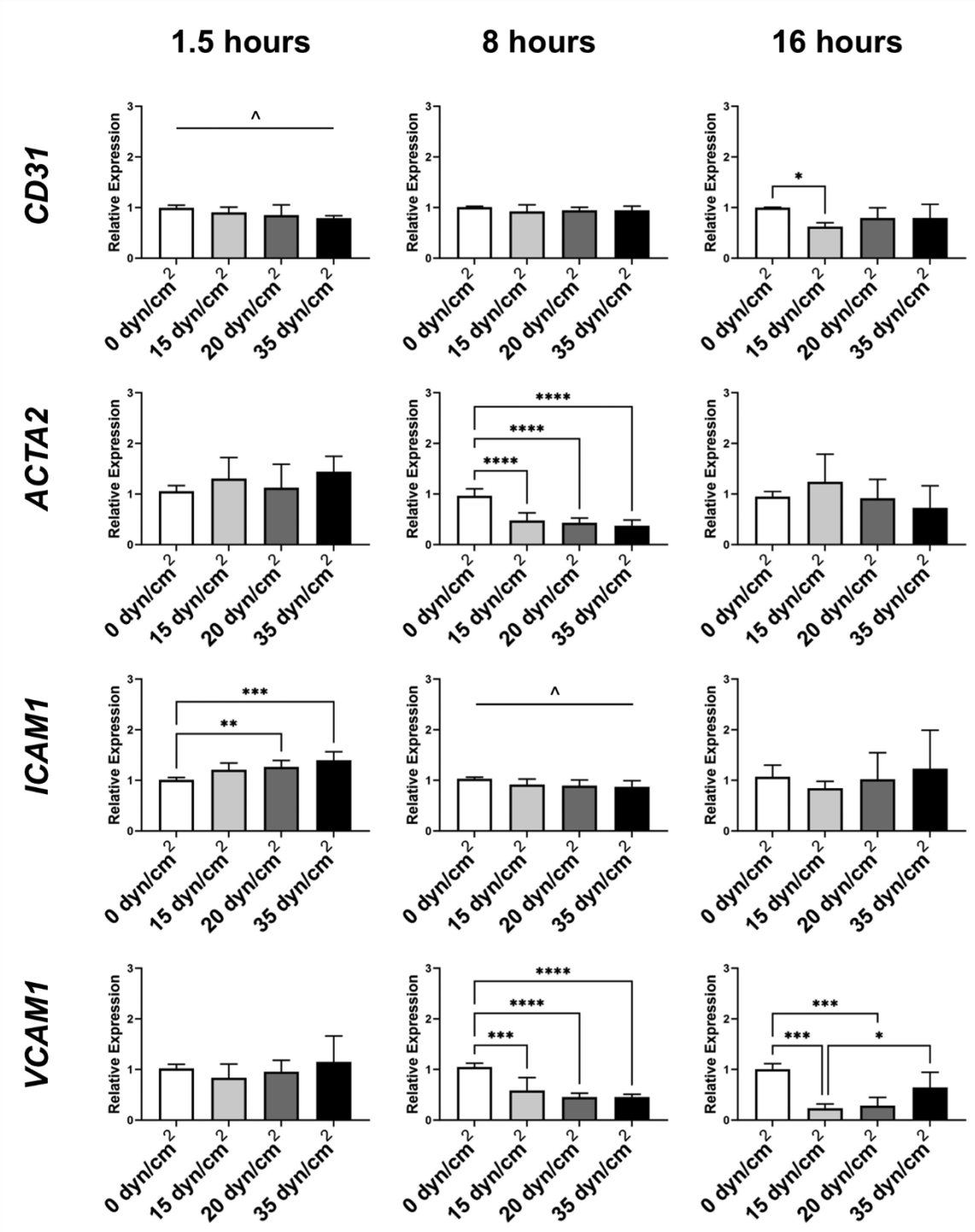

Figure 3. Gene expression of *CD31*, *ACTA2*, *ICAM1*, and *VCAM1* by EECS under static conditons and 15-35 dyn/cm^2 conditions for 1.5, 8, and 16 hours. N=3. Data was normalized to the static condition for each time point, analyzed by one-way ANOVA, and expressed as mean ± SD. *p=0.01-0.05, **p=0.001-0.01, ***p=0.0001-0.001, ****p<0.0001.

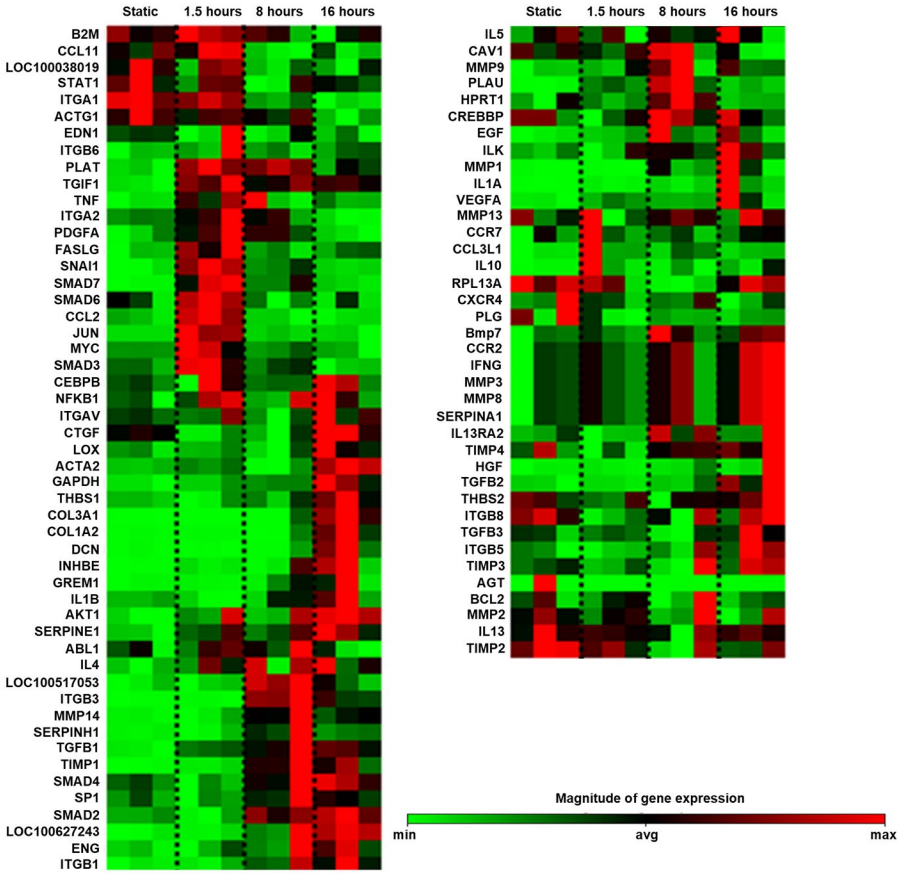

Figure 4. Fibrosis profiler array comparing the gene expression of static EECs to EECs exposed to high shear stress at 1.5, 8, and 16 hours, respectively. The samples are grouped by shear condition and time point. A separate z-distribution is shown for each gene. Green = minimum magnitude of gene expression; Red = maximum magnitude of gene expression.

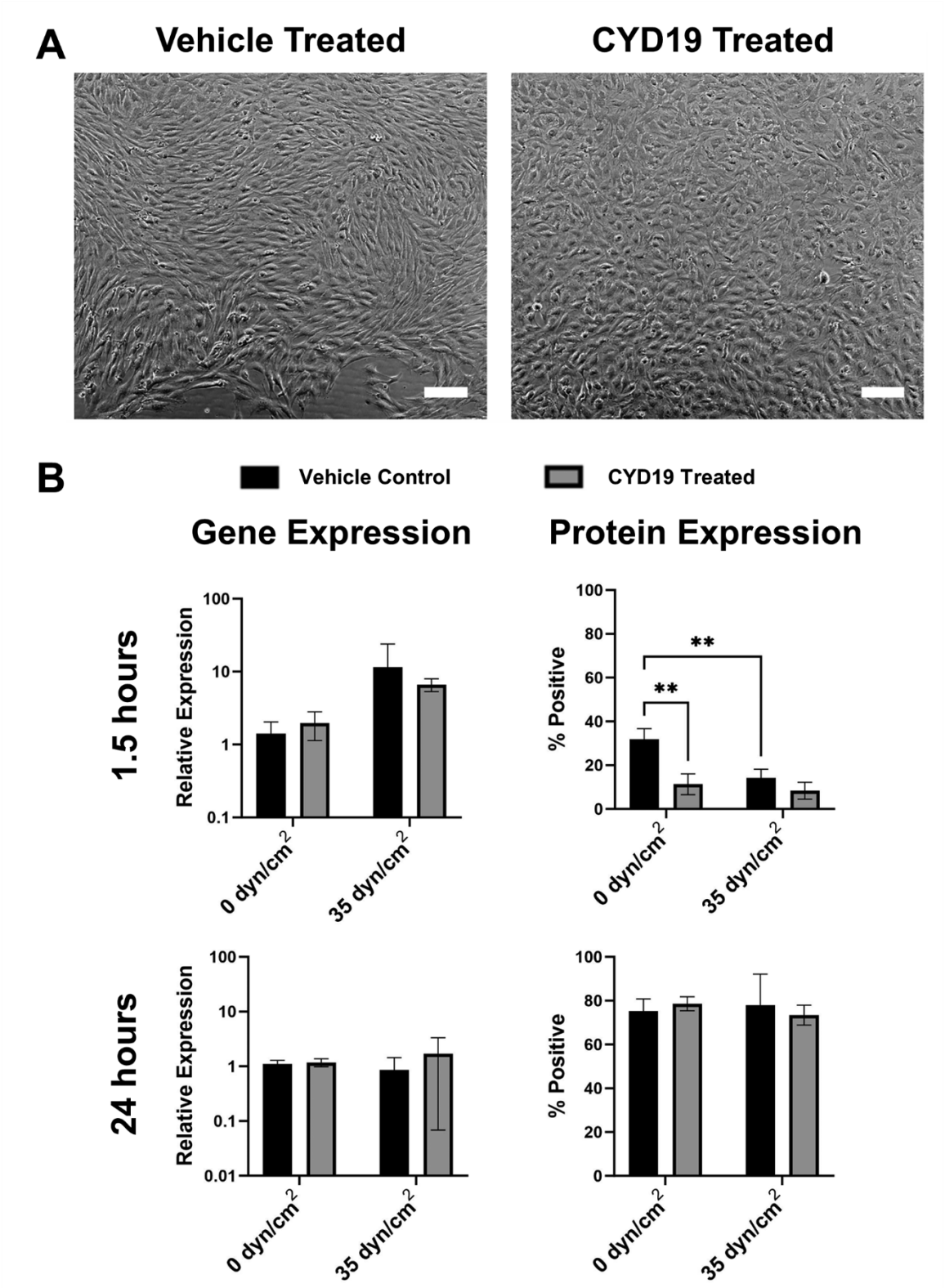

Figure 5. (A) Comparison of vehicle-treated EECs (left) and CYD19-treated EECs (right). Scale bar = 100 µm. **(B)** Gene and protein expression of Snail from EECs cultured under either static conditions or high shear stress, and treated with either vehicle control or the small molecule inhibitor CYD19 at 1.5 hours and 24 hours. Data is expressed as mean ± SD. *p=0.01-0.05, **p=0.001-0.01, ***p=0.0001-0.001, ****p<0.0001.

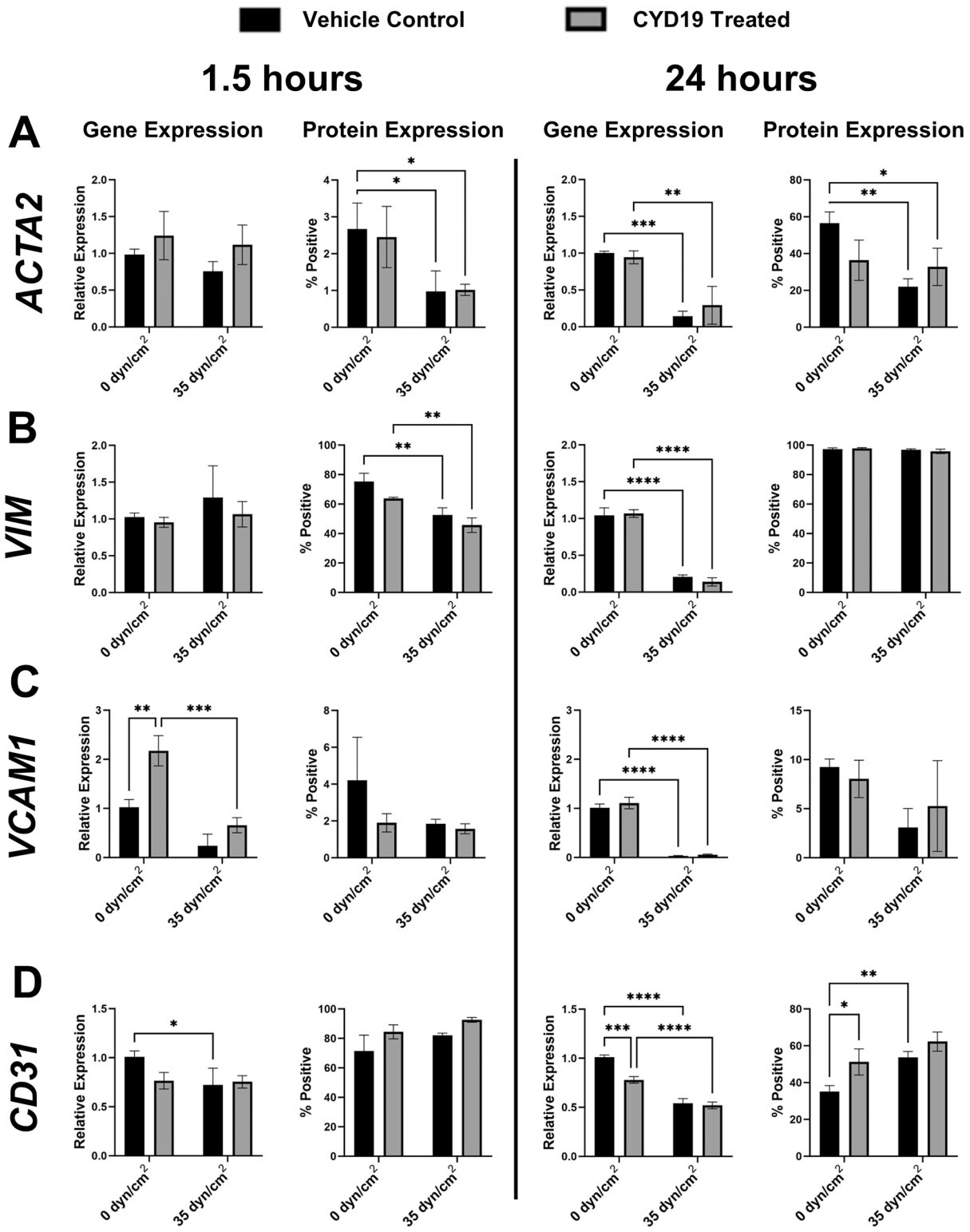

Figure 6. Gene and protein expression of (A) α-smooth muscle actin, (B) vimentin, (C) VCAM1, and (D) CD31 from EECs cultured under either static conditions (0 dyn/cm^2) or high shear stress (35 dyn/cm^2), and treated with either vehicle control or the small molecule inhibitor CYD19 at 1.5 hours and 24 hours. Data is expressed as mean ± SD. *p=0.01-0.05, **p=0.001-0.01, ***p=0.0001-0.001, ****p<0.0001.

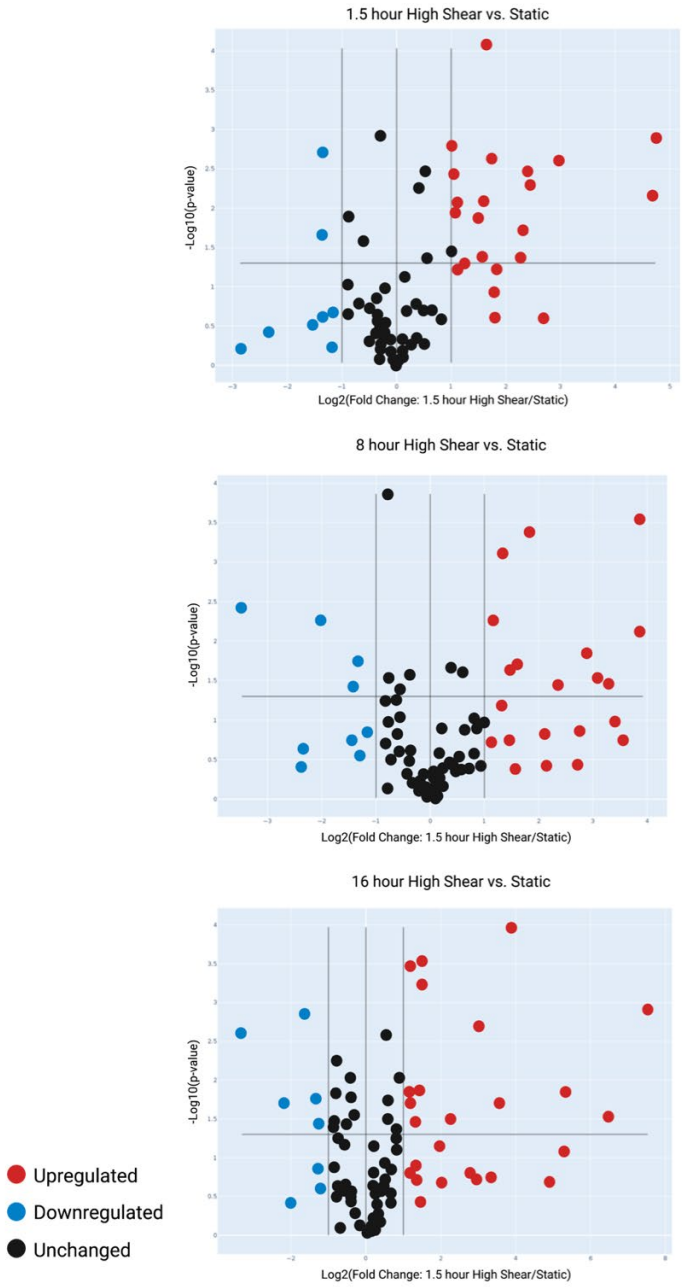

Supplemental Figure 1. Volcano plots comparing the gene expression of static EECs to EECs exposed to high shear stress at 1.5, 8, and 16 hours, respectively. Genes that are significantly upregulated are shown as red dots, genes that are significantly downregulated are shown as blue dots, and genes that remain unchanged are shown as black dots.